Article

J. Mex. Chem. Soc. **2025**, *69*(1)
Special Issue

ISSN-e 2594-0317

The Effect of *bcc* lattices on the Drug Release Kinetics in Inert Systems by Monte Carlo Simulation

Saúl Jiménez-Jiménez[1], Salomón Cordero-Sánchez[2*], Rafael Villalobos García[1*], J. Gerardo Mejía-Hernández[1], Juan Villegas-Cortez[3]

[1]Laboratorio de Investigación y Posgrado en Tecnología Farmacéutica, Facultad de Estudios Superiores Cuautitlán, Universidad Nacional Autónoma de México, Av. 1o de Mayo s/n, Santa María las Torres, Cuautitlán Izcalli, Estado de México, México, C.P. 54740.

[2]Departamento de Química, Universidad Autónoma Metropolitana-Iztapalapa, Ciudad de México 09310, México.

[3]Departmento de Sistemas, Universidad Autónoma Metropolitana, Av. Sn. Pablo 420, Col Nueva El Rosario, CP 02128, Alc Azcapotzalco, Mexico City, Mexico.

***Corresponding author:** Salomón Cordero-Sánchez, email: scordero@izt.uam.mx; Rafael Villalobos-García, email: rafael2f2@gmail.com

Received May 25th, 2024; Accepted September 25th, 2024.

DOI: http://dx.doi.org/10.29356/jmcs.v69i1.2295

Abstract. This study examines the release kinetics of hydrophilic drugs from inert and porous matrices structured as body-centered cubic (*bcc*) lattices, utilizing Monte Carlo simulations for analysis. In this research, we examined a sphere with three distinct radii and a cylinder with three varying height-to-radius ratios. For each sample, we assessed the kinetics of drug release at varying drug concentrations and modeled the release by simulating the random diffusion of drug particles to the device's boundaries. The comparison of release profiles highlighted the influence of size, geometry, and connectivity on the kinetic parameters and essential properties. Enhancing the area-to-volume ratio leads to a diminished rate of drug release. Similarly, an escalation in size, as indicated by the ratio 1:18:55, results in a reduced drug release rate. Additionally, our findings reveal that the quantity of drug retained indefinitely is greater within a body-centered cubic (*bcc*) lattice matrix compared to a simple cubic (cs) lattice structure. In both geometrical configurations, the trapped drug is independent of the system's scaling in comparison to a *cs* lattice. Furthermore, our analysis reveals that at larger scales, with a drug concentration above the theoretical percolation threshold, our system remains stable. The outcomes align with the empirical Higuchi equation and the Weibull function. Our findings concur with previously published experimental outcomes, suggesting that *bcc* connectivity is a reliable parameter for simulating diffusion processes in the drug release from solid pharmaceutical forms. This correlation supports the use of *bcc* connectivity as a predictive tool in pharmaceutical research, aiding in the understanding of drug release mechanisms.
Keywords: Drug release kinetics; diffusion; connectivity; Monte Carlo simulation; Weibull function; Higuchi function; *bcc* lattice.

Resumen. Este trabajo analiza la cinética de liberación de fármacos hidrófilos a partir de matrices inertes y porosas en una red cúbica centrada en el cuerpo (*bcc*) mediante simulacion de Monte Carlo. Para este estudio, seleccionamos una esfera con tres radios diferentes y un cilindro con tres relaciones altura/radio diferentes. Para cada uno, determinamos la cinética de liberación del fármaco con diferentes cargas y simulamos la liberación a través del movimiento aleatorio de cada partícula del fármaco hacia los límites del dispositivo mediante un proceso de difusión. Se compararon los perfiles de liberación y analizamos el efecto de

J. Mex. Chem. Soc. **2025**, *69*(1)
Special Issue

ISSN-e 2594-0317

escalamiento, la geometría y la conectividad sobre los parámetros cinéticos y las propiedades críticas del sistema. Al aumentar la relación área/volumen, disminuye la tasa de liberación del fármaco, mientras que con el aumento del tamaño (1:18:55), la tasa de liberación del fármaco disminuye. Además, identificamos que la cantidad de fármaco atrapado a tiempo infinito es mayor en la matriz constituida por la red *bcc* que en la red cúbica simple (*cs*). En ambas geometrías, bajo una red *bcc* se observó que la cantidad de fármaco atrapado no es sensible al escalamiento del sistema en comparación con una red *cs*. Además, caracterizamos nuestros sistemas mostrando que en escalas mayores y con una carga de fármaco muy por arriba del umbral de percolación teórico, los datos se ajustan a la ecuación empírica de Higuchi y la función de Weibull. Nuestros datos concuerdan resultados experimentales y teóricos previamente reportados, lo que permite considerar la conectividad *bcc* como un buen parámetro de simulación de procesos difusivos, como la liberación de fármaco desde formas farmacéuticas sólidas.
Palabras clave: Cinética de liberación de fármacos; difusión; conectividad; simulación Monte Carlo; función Weibull; función Higuchi; red *bcc*.

Introduction

The release of a drug from a pharmaceutical dosage form is a pivotal stage to achieve a desired therapeutic response. It occurs when the drug, initially embedded in a solid form, encounters a liquid environment. This contact triggers the drug's dissolution and the ensuing dispersion from its solid matrix, like a tablet, into the body [1]. Diffusion plays a pivotal role in the release of drugs, driving the migration of molecules from areas of higher to lower concentration. Utilizing Monte Carlo simulations, a method grounded in probability, enhances our comprehension of this phenomenon. This technique facilitates the examination of diverse conditions and forecasts the kinetics of drug release with improved precision. By simulating molecular randomness, these models shed light on the underlying processes of drug release, which is crucial for crafting effective drug delivery systems. By combining the principles of diffusion with computational modeling, scientists are able to enhance drug delivery mechanisms, ensuring more effective therapeutic results [2-5]. For example, this class of computational procedures have allowed provide insights into the mechanisms of drug release that are essential for the development of controlled-release pharmaceuticals [6-9]. Simulations can help in in identifying key characteristics like the percolation threshold, crucial for refining drug delivery systems [10-14]. In porous mediums, the percolation threshold is a vital principle, especially relevant in disciplines such as hydrology, environmental engineering, and materials science. It denotes the essential juncture where a substance, such as a pharmaceutical, attains a level of concentration sufficient to create an unbroken pathway through the material, thus facilitating effective penetration or movement within the system. Understanding the concept of the percolation threshold is crucial for enhancing processes such as filtration, establishing barriers, and managing drug delivery in various industrial and scientific fields [15]. The percolation threshold plays a key role in analyzing porous structures and can be measured through different experimental techniques [17-20]. One effective approach is to evaluate the drug release pattern to derive the constant for the Higuchi equation, which can then be linked to the ultimate porosity of the system [21]. The percolation threshold is a critical concept in the formulation of drug delivery systems, serving as a key indicator of the robustness of a drug's release profile. It is determined by analyzing kinetic parameters alongside mechanical, physicochemical, and rheological data, which can predict how a drug or excipient behaves within a specific formulation [15,18,20-25]. Fractal theory provides a method to calculate the percolation threshold by estimating the fractal dimension, which reflects the complexity of the porous structure [26]. Additionally, the fraction of a drug trapped indefinitely within an inert matrix (Q_t) can be used to estimate the percolation threshold, considering the initial drug load (C_0) [16]. In computational simulations, the coordination number significantly influences the release kinetics of particles within a lattice structure. This parameter dictates the number of nearest neighbors each particle can interact with, which in turn affects the particle's ability to migrate or be released from the device. Therefore, selecting an appropriate lattice connectivity is crucial for accurately modeling the release kinetics and predicting the behavior of particles in various applications, from drug delivery systems to material

J. Mex. Chem. Soc. **2025**, *69*(1)
Special Issue

ISSN-e 2594-0317

science [27]. The percolation threshold is influenced by the system's dimension (*d*) and the lattice connectivity (*c*) [28]. The relationship between lattice connectivity and the percolation threshold is indeed a subject of scientific inquiry. Research indicates that the inverse of the percolation threshold tends to have a linear relationship with the lattice coordination number, suggesting a similarity in percolation clusters across different coordination numbers [29]. However, as coordination values of lattices approach each other, the nature of this relationship can become more complex, leading to debates within the scientific community [30]. *cs* lattices are indeed a staple in drug release simulations due to their straightforward structure, which allows for the study of diffusion-based release mechanisms [11,31]. However, the limitation of having only six neighbors restricts the complexity of models that can be constructed, particularly those requiring dynamic connectivity [32]. The drug release process is a complex interplay of various phenomena, where phase transition, polymorphism, and particle solvation play critical roles. For example, changes in the polymorphic form of a drug can modify how quickly it dissolves and is absorbed by the body, which can affect the drug's effectiveness in treatment [33]. Similarly, the solvation of particles during drug release can influence the drug's solubility and, consequently, its bioavailability. Therefore, analyzing these phenomena as changes in the connectivity of the drug release device can provide valuable insights into optimizing drug delivery systems [34]. Considering the diverse processes that can occur during the release of a drug, which are shaped by the design of the formulation, the aspect of connectivity emerges as a key element. It can significantly impact the predictions of drug release kinetics and key parameters such as the percolation threshold. This highlights the importance of considering connectivity in the design and analysis of drug delivery systems [35-37]. However, lattice connectivity remains an underexplored parameter for analyzing the kinetics of drug release from drug delivery systems. In this research, we explore the site percolation threshold for a *bcc* lattice considering the impact of scale size. A *bcc* lattice is created by inserting an additional lattice point at the center of every cubic cell within a *cs* lattice. This arrangement results in eight lattice points located at the corners of each cubic cell. The *bcc* lattice configuration is particularly useful for simulating systems where each lattice point is surrounded by eight neighboring cubic cells, with the central point of each cubic cell being unique to that cell alone [38]. Examining this set of parameters within the Monte Carlo simulation may yield novel methods for predicting thermodynamic variations that arise from altering connectivity as various mechanisms are modeled in tandem.

The subsequent sections of this paper detail the methodology employed to simulate drug release from inert matrices structured as *bcc* lattices. This is followed by an analysis and discussion of how geometry influences the drug release profile and kinetics. The paper concludes with a summary of our findings.

Methodology

The suggested model illustrates a binary system composed of an inert excipient and a hydrophilic drug. The simulation was conducted for hydrophilic drugs that demonstrate immediate dissolution upon contact with aqueous solutions. In the simulation of the drug delivery system, we established two geometric models: one shaped like a sphere and another resembling a cylinder with flat ends. The spherical model was characterized solely by its radius (*R*), while the cylindrical model was described by both its height (*H*) and radius (*R*) (Fig. 1). In the configuration, each system is positioned at the center of the cube, with coordinates (*L/2, L/2, L/2*). The initial volume is denoted as $V_{device} = V_{i,t0}$, in accordance with the data presented in Table 1. In the model, each location, denoted as (*i,j,k*), is linked through a standardized *bcc* lattice structure, and is categorized either as a drug or an excipient. The composition of each system includes an initial concentration of the drug, labeled as (C_0), which represents the proportion of the lattice sites filled with dry drug particles, expressed as $C_0 = X_{drug}V_{device}$ at the start of every simulation *t(0)* and where X_{drug} represents the fraction of sites with drug. The drug and the excipient are distributed through a process of randomization. Upon defining the cubic lattice vectors, one can proceed to construct a spherical matrix. This matrix is defined by the set of coordinates that satisfy the equation, $x^2 + y^2 + z^2 < R^2$. Concurrently, a cylindrical device is defined by two conditions: the axial coordinate *z* must either be less than (*L/2 + H/2*) or greater than (*L/2 + H/2*), and the radial coordinates must satisfy $\left(x - \frac{L}{2}\right)^2 + \left(y - \frac{L}{2}\right)^2 < R^2$. Upon initial

J. Mex. Chem. Soc. **2025**, *69*(1)
Special Issue

ISSN-e 2594-0317

contact with water in the simulation, drug particles dissolve and relocate, whereas the excipient remains stationary throughout the delivery process. In these simulations, drug particles are depicted as random walkers, randomly selecting one of eight possible directions provided by a *bcc* connectivity to potentially move to an adjacent site. If the movement criteria are met, the particle will transition to the new site; otherwise, it remains stationary. Each movement attempt, irrespective of its outcome, advances the simulation clock by an amount inversely proportional to Nt. Here, Nt represents the total number of drug particles within the matrix at time t, and time is measured in arbitrary units known as Monte Carlo Steps [39-41]. Under the specified conditions, the drug particle will keep moving until it exits the spherical matrix device, defined by the equation $x^2 + y^2 + z^2 \geq R^2$. In the case of a cylindrical matrix, the drug is released once the particle has moved beyond either the axial or the radial boundaries. The experiment was conducted 500 times, recording the average number of drug particles released, along with the standard deviations. The drug release algorithm was implemented consistently until a stable rate of drug release was achieved.

The fraction of the drug released, represented as M_t/M_0, is calculated from the quantity of drug particles released in each simulation and then analyzed through the following equations. In Eq. (1), M_t denotes the amount of drug released at time *t*, and M_0 signifies the total drug amount . The kinetic constants *a* and *b* were determined using the Weibull model for analysis.

$$\frac{M_t}{M_0} = 1 - \exp\left(-\mathrm{a}t^b\right) \tag{1}$$

This approach involved assessing spheres of different dimensions, with radii of measuring 10, 26 and 38 lattice units. Similarly, cylinders with a radius of 10, 26 and 38 lattice units and a height of 13, 35, 51 units respectively were also analyzed, as illustrated in Fig. 1. On the other hand, the estimation of the percolation threshold value was conducted using the method proposed by Villalobos et al., 2005 [31]. The percolation threshold is determined by calculating the quantity of drug entrapped, denoted as Q_t, within the system. This is subsequently matched against the cumulative probability of a normal distribution to estimate its own cumulative probability. The formula for this expression is as follows:

$$Q_t = a + aErf[b(-\varepsilon_c + \varepsilon)] \tag{2}$$

where *Erf* refers to the error function. The constants *a* and *b* are parameters specific to the process, ε signifies the initial quantity of the drug, and ε_c is indicative of the critical percolation threshold of the drug. Rewriting the equation above, we define the change in the accumulated drug quantity relative to the initial drug quantity as follows:

$$\frac{dQ_t}{d\varepsilon} = -\frac{2ab}{\sqrt{\pi}} e^{\left[-b^2(-\varepsilon_c+\varepsilon)^2\right]} \tag{3}$$

The inflection point on the cumulative probability curve indicates a shift in the relationship between the accumulated drug quantity and the initial drug amount, corresponding to the condition where $-\varepsilon_c + \varepsilon = 0$. At this stage, a percolating cluster has been established, signifying that the threshold for drug percolation has been reached. By applying non-linear regression to the preceding equation, we can identify the function that characterizes this behavior and pinpoint the peak value, which signifies the percolation threshold [31].

Q_t, the proportion of the drug that is encapsulated within the inert structure is expressed as:

$$Q_t = 1 - \frac{M_\infty}{N_0} = 1 - Q_c \tag{4}$$

where Q_c represents the cumulative quantity of the drug released when time approaches infinity (M_∞), which is then divided by the initial count of drug particles present within the matrix (N_0) at the start of

J. Mex. Chem. Soc. **2025**, *69*(1)
Special Issue

ISSN-e 2594-0317

the experiment. To determine M_∞, we formulated an algorithm that identifies the isolated dry drug clusters remaining within the system. Upon initialization at the surface, the system undergoes a transformation each time it contacts a drug particle, resulting in its modification to a water-based environment. In time, the entire system will become infused with water particles, with the exception of those particles that do not aggregate into clusters externally. In each cycle, the quantity Q_t can be tallied up to a total of N_0 steps. (Fig. 1). All of these algorithms have been implemented using the ANSI C language.

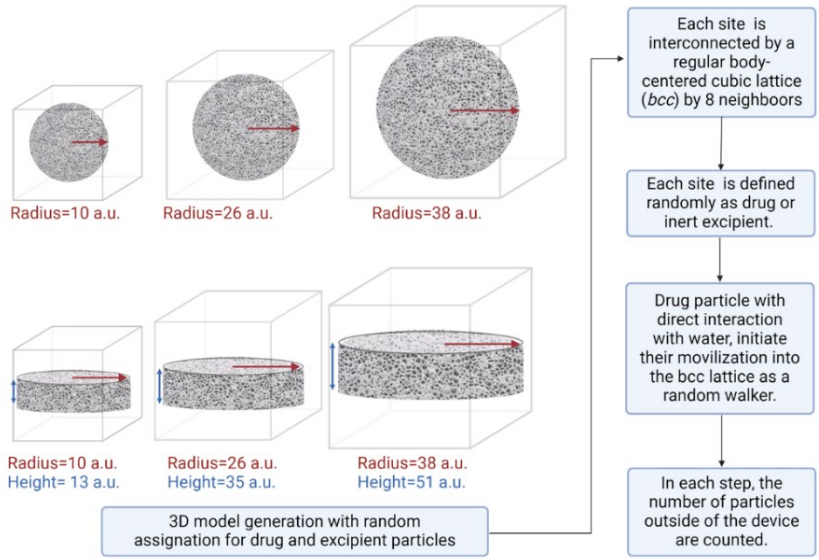

Fig. 1. Schematization of the Monte Carlo simulation methodology used in this work. The term a. u. stands for arbitrary units.

Results and discussion

Influence of geometry and size on the drug release profile

Our study began by generating drug release profiles at various hydrophilic drug loading levels, as shown in Table 1. The theoretical composition of the components in this system is expressed as solute volume with respect to the initial volume of each component in percentage (%v/v). For the drug, C_0 is calculated as the percentage of volume of drug particles in the system with respect to the initial drug volume. At the beginning of the simulation at t(0) the C_0 in the device is calculated as $C_0=X_{drug}V_{device}$, where X_{drug} represent the drug fraction and V_{device} stands for the volume of the system.

Subsequently, we determined the percolation threshold by applying the methodology suggested by Villalobos et al. in 2005 [31].

J. Mex. Chem. Soc. **2025**, *69*(1)
Special Issue

ISSN-e 2594-0317

Table 1. Parameter values for the dissolution of a drug across various geometries and sizes, utilizing a connectivity model based on a *bcc* lattice.

Descriptors	**Geometry**	**Parameter simulated**	**Model 1**	**Parameter simulated**	**Model 2**	**Parameter simulated**	**Model 3**
Volume calculated (C_0)	Sphere	Radius: 10 a.u.	4187	Radius: 26 a.u.	73585	Radius: 38 a.u.	229731
	Cylinder	Radius: 10 a.u. Height: 13 a.u.	4082	Radius: 26 a.u. Height: 35 a.u.	74292	Radius: 38 a.u. Height: 51 a.u.	231243
Surface área (a.u.^{2})	Sphere	Radius: 10 a.u.	1256	Radius: 26 a.u.	8491	Radius: 38 a.u.	18137
	Cylinder	Radius: 10 a.u. Height: 13 a.u.	1444	Radius: 26 a.u. Height: 35 a.u.	9960	Radius: 38 a.u. Height: 51 a.u.	21239
Area/volume ratio (a.u.$^{-1}$)	Sphere	Radius: 10 a.u.	0.2768	Radius: 26 a.u.	0.1154	Radius: 38 a.u.	0.0789
	Cylinder	Radius: 10 a.u. Height: 13 a.u.	0.3537	Radius: 26 a.u. Height: 35 a.u.	0.1340	Radius: 38 a.u. Height: 51 a.u.	0.0918

J. Mex. Chem. Soc. **2025**, *69*(1)
Special Issue

ISSN-e 2594-0317

Our research details the drug release profiles from both cylindrical and spherical shapes, which, despite having identical volumes, vary in *A/V* ratio. The release profile was first depicted by plotting the percentage of drug released over the initial drug load (M_t/M_0) against time (t). The results confirm that a decrease in the surface area-to-volume (A/V) ratio accelerates the release rate in both shapes, with the spherical geometry exhibiting a notably quicker release than the cylindrical one, as illustrated in Fig. 2. The study confirms that an increased surface area changes how substances are released, with cylindrical shapes showing greater efficiency than spherical ones. Additionally, the research reveals a predictable trend: for a given shape, the rate at which a drug is released decreases as the size of the shape increases. The surface area of drug formulations is crucial in dictating the kinetics of drug release, particularly under a Fickian diffusion process [42-45].

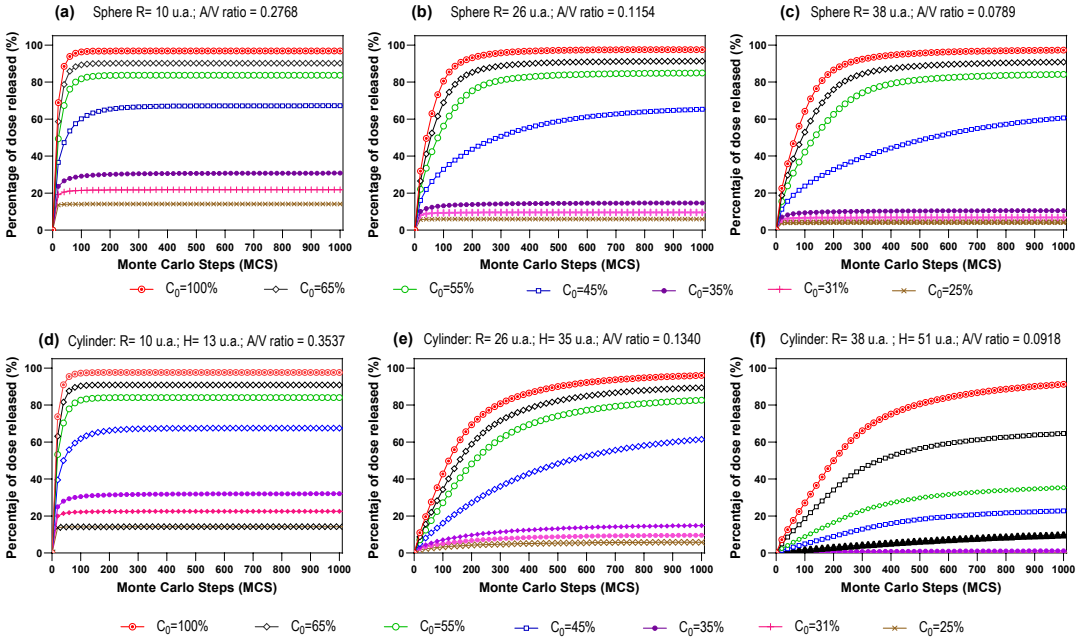

Fig. 2. Drug release profiles from a variety of solid, inert geometries linked via a body-centered cubic (*bcc*) lattice, which differ in their initial drug load and the ratio of surface area to volume. **(a-c)** Top row: spherical geometry. **(d-f)** Bottom row: cylindrical geometry.

Extensive research suggests that spherical shapes release substances more quickly than cylindrical ones, with surface area playing a crucial role in the rate of release [45]. It has been observed that systems containing a higher concentration of a drug typically exhibit a quicker release than those with less. Analytical studies have reinforced this relationship, revealing that an increase in drug quantity correlates with an accelerated release rate [46]. As the system size varies, the release rate diminishes in proportion to the system's dimensions. Our findings indicate a strong correlation between the release rate and the quantity of drug retained indefinitely, showing that both percolation and particle size significantly influence the drug's release process. This is especially pronounced in shapes with a smaller surface area, such as spheres compared to cylinders (Fig. 3 and Fig. 6**(a)**).

Upon examining the drug release profiles from different lattice structures (Fig. 5**(a)** and Fig. 5**(b)**), it has been noted that when drug concentrations go beyond the theoretical percolation threshold of 0.24 for a *bcc* lattice [50-52], the resulting release rate exceeds that observed in a *cs* lattice, as illustrated in Fig. 6**(b)** and Fig. 6**(c)**. If the drug concentration falls below the percolation threshold, it remains trapped and unable to reach the surface. This leads to a diminished release of the drug over an extended period, suggesting the presence of an anomalous release mechanism. Both geometries exhibit comparable behaviors; however, the release rates in cylindrical geometry decline more swiftly than those in a solid, inert sphere (Fig. 6**(b)** and 6**(c)**). Additionally, when C_0 exceeds P_c, there is a corresponding decrease in the release rate as the particle count C_0 diminishes (Fig. 2). In the

J. Mex. Chem. Soc. **2025**, *69*(1)
Special Issue

ISSN-e 2594-0317

cylindrical model, the impact of size on the rate of released drug is more pronounced than in the spherical model, particularly near the percolation threshold. This suggests that the volume increase and the consequent rise in particle generation significantly influence the rate of release [44-46]. The constructed simulation model utilizes the free volume theory. This theory posits that the solute, in this case, a hydrated drug, moves dynamically through vacant or available spaces among particles. This movement is not influenced by interaction, as there is free volume present for the drug to occupy, facilitating the gradual development of a percolating network [47-48]. The initial contact of water with dry drug particles sets off a process where the particles dissolve, starting the formation of the percolating network, which is contingent on the number of exposed sites and the system's geometry. Thus, a *bcc* lattice structure will allow a higher water uptake compared to a *cs* lattice, resulting in a larger quantity of drug being available for release. This accounts for the observed higher release rate from a *bcc* lattice when compared to a *cs* lattice, provided that the diffusivity remains constant in both structures.

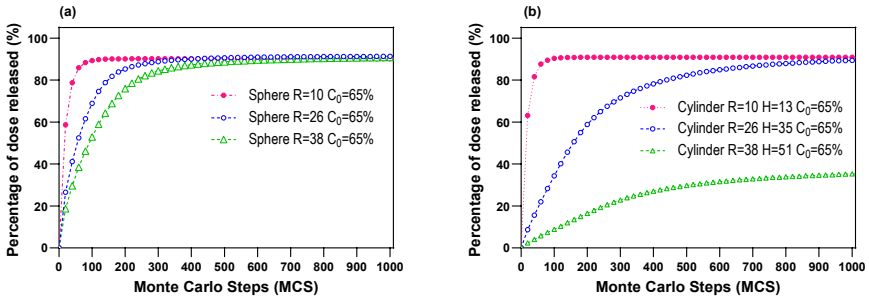

Fig. 3. Impact of size scaling on drug release profiles within **(a)** spherical and **(b)** cylindrical geometries when the drug concentration exceeds the percolation threshold.

Impact of Body-Centered Cubic (*BCC*) structure on the drug release profile

In a system based on a *bcc* lattice, our data show a distinct release rate when compared to a simple cubic lattice (Fig. 4). Furthermore, each type of lattice demonstrates a unique pattern of convergence for the amount of drug released over an infinite period (Fig. 5**(a)** and Fig. 6**(a)**). Our study revealed that drug release rates are more rapid in a *bcc* lattice compared to a *cs* lattice, with consistent patterns across different shapes. Notably, in the case of *bcc* structures, the average values derived from 500 samples quickly reached a steady state, marked by M_∞, yielding an estimation with a high degree of precision, as indicated by a standard deviation of less than 5 %. The sample size is consistent with the accurate estimation of the first statistical moments, including mean and variance, as observed in various Monte Carlo studies. These studies analyze diffusion processes in models that replicate a porous medium, aiming to reach a stable state of higher-order statistics [53].

In a preceding study conducted on a *cs* lattice, the threshold for hard spheres was identified at 0.3116 (Represented in Fig. 5**(c)**) similar to cylinder (Fig. 5**(b)**), whereas for an analogous system in a *bcc* lattice, the estimated threshold value was determined to be around 0.45 for cylinders and 0.38 for spheres (Fig. 6**(b)** y 6**(c)**, respectively). The deviation of our findings from the expected theoretical values can be attributed to factors such as finite size effects, the degree of connectivity, and the dynamics of water uptake. It should be noted that the methodology employed to determine the percolation threshold ensures that any drug particle not linked to the tablet's exterior maintains a standard cumulative probability. Should this assumption be invalidated, the results could be skewed, with a greater potential for deviation when the quantity of the drug remaining isolated at infinite time is substantial. Similarly, additional factors such as the behavior of random number generators and the governing rules of the random walker can influence the accuracy of the percolation threshold estimation [52-53]. Alternative methods for determining the percolation threshold in three-dimensional lattices are limited to datasets that align well with the Higuchi equation [21] or those conducted on Bethe lattices [54]. This method demonstrates that using *bcc* lattices, one can discern the influence of a device's geometry on the percolation threshold calculation. It reveals that when the A/V ratio is low (Table 1), the percolation threshold decreases (Fig. 6**(b)** and Fig. 6**(c)**). Additionally, it indicates that for spherical geometries, the initial drug load required to form a percolating cluster is minimal and yields a more interconnected structure. Numerous research efforts have established how lattice types affect dynamic characteristics

J. Mex. Chem. Soc. **2025**, *69*(1)
Special Issue

ISSN-e 2594-0317

at critical points. For instance, it has been found that a system with enhanced connectivity can lead to a change in the rate of diffusion [55]. The variation in percolation threshold values can be attributed to the greater amount of free space found in a simple cubic structure, which has a different packing factor, in contrast to a *bcc* structure that has a higher packing factor. The *bcc* lattice is a regular structure with a coordination number of 8. For a linear dimension L, it possesses 3/4L vertices and 3L edges, which facilitates drug diffusion. Consequently, the percolation threshold is lower compared to a *cs* lattice with identical structure and composition [56,57]. In studies similar to those on other critical values, it has been observed that enhanced connectivity leads to a decrease in these values. This decline can be attributed to the heightened likelihood of movement within a more interconnected lattice. Essentially, as the network becomes more integrated, the critical values tend to diminish accordingly [58].

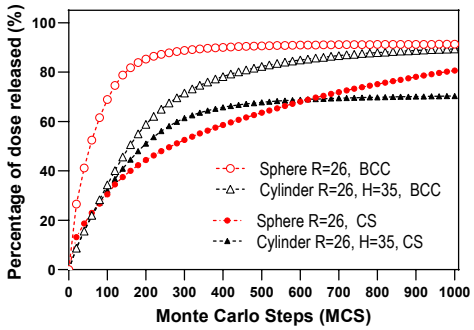

Fig. 4. Effect of the coordination number on drug release profiles for two distinct geometries using a drug load within both *bcc* and *cs* lattices and above of the respective percolation threshold values (C_0=65 %).

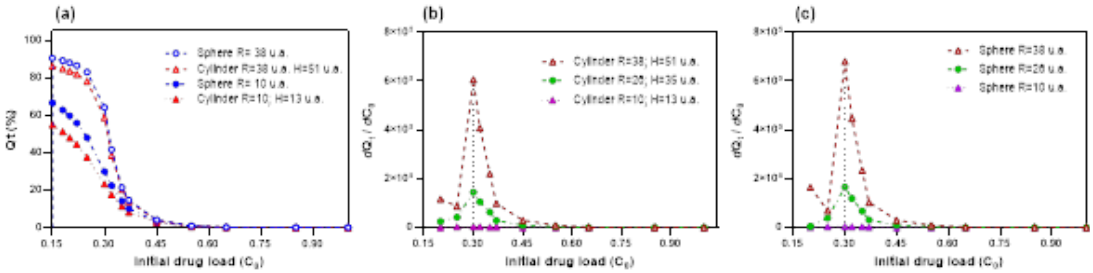

Fig. 5. (a) Release values, representing the average of 500 simulations, for both spherical and cylindrical devices, an infinite time point using a *cs* lattice. Dose retention rate in cylindrical devices of varying dimensions utilizing *cs* lattices and determination of the percolation threshold through extrapolation: **(b)** cylindrical devices; **(c)** spherical devices.

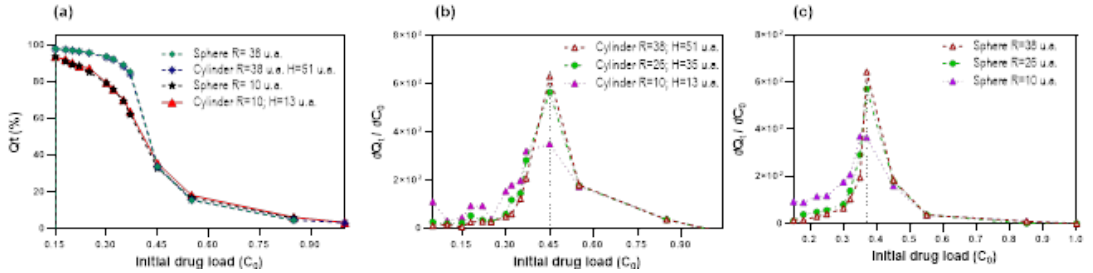

Fig. 6. (a) Release values, representing the average of 500 simulations, for both spherical and cylindrical devices, at infinite time point using a *bcc* lattice. Dose retention rate in devices of varying dimensions utilizing *bcc* lattices and determination of the percolation threshold through extrapolation: **(b)** cylindrical devices; **(c)** spherical devices.

J. Mex. Chem. Soc. **2025**, *69*(1)
Special Issue

ISSN-e 2594-0317

Kinetic analysis

Following the analysis of drug release profiles, kinetic constants were derived to identify the governing mechanism of release across various geometries, drug concentrations, and scales. The analysis of the data using Higuchi's equation demonstrated a satisfactory fit for initial drug loads of 0.45 or higher (Table 2). In a manner akin to observations in *cs* lattices, when the drug load is beneath the calculated *bcc* critical threshold, the data fail to conform to the square root law of the Higuchi model. When the values exceed the estimated critical point, the R^2 coefficient demonstrates a robust adjustment, particularly under conditions of high loads and increased volumes. In this study, data analysis was conducted manually, focusing solely on the inflection curve, and when around 60% of the drug release was achieved. The model tended to overestimate the fraction of the drug released. Generally, the data curves align well with the Higuchi model, indicating that the release process is likely governed by Fickian diffusion. In cylindrical geometries where the A/V ratio is high, the resulting *b* value suggests Fickian diffusion. Yet, when approaching the percolation threshold, this constant exhibits characteristics of anomalous diffusion. Finally, through this analysis it is observed a good agreement between Higuchi and Weibull model for the drug release above of the percolation threshold estimated.

Table 2. Kinetic analysis of drug release applying the Higuchi and Weibull models for two distinct geometrical configurations. Size system refers to the volume of the system that is equal to the sum of total particles of each component (% excipient volume + % drug volume) at the beginning of the simulation at *t(0)*. M_t is the percentage of drug released at time t with respect to the initial volume of drug in the system; M_0 is the percentage of drug in the system at time *t(0)*; K_H represents the Higuchi release kinetic constant.

Drug content	Size (Volume)		Higuchi model $\frac{M_t}{M_0} = kt^{0.5}$				Weibull model $\frac{M_t}{M_0} = 1 - \exp(-at^b)$			
	Sphere	Cylinder	Sphere		Cylinder		Sphere		Cylinder	
	Volume	Volume	K_H	R^2	K_H	R^2	b	R^2	b	R^2
1.0	4187	4082	7.8870	0.9980	7.590	0.9975	0.3810	0.9100	0.5700	0.9095
	73585	74292	6.3211	0.9983	5.2301	0.9950	0.7095	0.9945	0.7567	0.9968
	229731	231242	6.8260	0.9913	4.8185	0.9993	0.7596	0.9981	0.7807	0.9969
0.85	4187	4082	7.8779	0.9756	7.753	0.9992	0.3510	0.7874	0.5190	0.9435
	73585	74292	6.2904	0.9967	4.4136	0.9984	0.7191	0.9923	0.7443	0.9994
	229731	231242	6.6554	0.9938	3.9671	0.9944	0.7008	0.9982	0.7968	0.9990
0.65	4187	4082	8.4509	0.9644	9.1335	0.9916	0.3358	0.7919	0.4834	0.9214
	73585	74292	7.2048	0.9950	3.2205	0.9983	0.6890	0.9945	0.7434	0.9785
	229731	231242	6.0454	0.9997	2.6792	0.9930	0.7500	0.9985	0.7970	0.9991
0.55	4187	4082	6.9175	0.9580	10.914	0.9832	0.3573	0.8486	0.3174	0.9542
	73585	74292	5.6108	0.9934	2.4615	0.9962	0.7515	0.9988	0.7742	0.9968
	229731	231242	4.9363	0.9997	1.8337	0.9982	0.7808	0.9980	0.7652	0.9900

J. Mex. Chem. Soc. **2025**, *69*(1)
Special Issue

ISSN-e 2594-0317

Drug content	Size (Volume)		Higuchi model $\frac{M_t}{M_0} = kt^{0.5}$				Weibull model $\frac{M_t}{M_0} = 1 - \exp(-at^b)$			
	Sphere	Cylinder	Sphere		Cylinder		Sphere		Cylinder	
	Volume	Volume	K_H	R^2	K_H	R^2	b	R^2	b	R^2
0.45	4187	4082	2.7903	0.9052	10.722	0.9552	0.3377	0.9560	0.3042	0.9468
	73585	74292	2.8512	0.9982	1.1871	0.9985	0.5195	0.9998	0.6287	0.9673
	229731	231242	2.2099	0.9997	0.7303	0.9918	0.5247	0.9996	0.7104	0.9674
0.35	4187	4082	0.5924	0.8539	2.4502	0.9252	0.1080	0.9222	0.1018	0.9117
	73585	74292	0.3579	0.8966	0.3316	0.9590	0.1334	0.9504	0.6087	0.9553
	229731	231242	0.2624	0.9008	0.2845	0.9700	0.1357	0.9525	0.6100	0.9660
0.31	4187	4082	0.2113	0.7529	0.8753	0.8482	0.0485	0.8446	0.0463	0.8393
	73585	74292	0.1199	0.7929	0.1314	0.9380	0.0594	0.8765	0.6149	0.8295
	229731	231242	0.0888	0.7998	0.0741	0.9571	0.0618	0.8812	0.5993	0.8521
0.25	4187	4082	0.3693	0.6221	0.1493	0.6992	0.0120	0.7274	0.0115	0.6968
	73585	74292	0.0204	0.6497	0.0628	0.9113	0.0150	0.7541	0.6104	0.7829
	229731	231242	0.0153	0.6496	0.0357	0.9570	0.0160	0.7540	0.5936	0.8059
0.15	4187	4082	0.0011	0.4405	0.0030	0.4816	0.0010	0.5439	0.0001	0.4816
	73585	74292	0.0006	0.5000	0.0020	0.5428	0.0010	0.6098	0.0014	0.7245
	229731	231242	0.0004	0.4924	0.0025	0.5960	0.0010	0.5978	0.0020	0.7529

Finally, in this model, we incorporated Class I biopharmaceutical drugs, which are characterized by their rapid solubility and high permeability. High permeability is indicative of the complete bioavailability of the drug fraction that is released. While the code can be modified to account for variations in solubility or the partition coefficient between water and solvent, this adjustment complicates the drug release algorithm and significantly increases the computational time required, often exponentially. Nevertheless, the approach to examine the solubility or distribution of the drug in octanol (log P) has been investigated using the Monte Carlo method. This technique has yielded results that align well with experimental data. For instance, Jorgensen et al. conducted an analysis of the solubility process and partition coefficient (log P), taking into account critical physical factors. These factor include the solute water Coulomb and Lennard-Jones interaction energies, as well as the solvent-accessible surface area, and the count of donor and acceptor hydrogen bonds [59]. In our model, the solubility of hydrophilic drugs is negligible due to the rapid solvation process, which achieves a saturated aqueous solution in equilibrium with the crystalline material in a relatively short time, and on a timescale much shorter compared to the release of drugs from pharmaceutical devices. For example, the analysis of complex molecules with multiple hydration sites shows a hydration process on the order of picoseconds, which, compared to the drug release process from controlled release systems, involves timescales on the order of hours

J. Mex. Chem. Soc. **2025**, *69*(1)
Special Issue

ISSN-e 2594-0317

or days [60]. Additionally, a model that integrates additional hydrodynamic phenomena, such as swelling and erosion processes, is particularly appealing for simulating poorly soluble drugs. This is because erosion or swelling often constitutes the rate-limiting step in the controlled release of the drug [61].

Conclusions

We have showed that applying the Monte Carlo method to a system structured by a *bcc* lattice can elucidate the experimental outcomes observed in systems akin to an inert matrix-type release mechanism. This is particularly applicable within a limited range when the initial drug load exceeds 0.45 by volume fraction for cylindrical shapes and 0.38 for spherical forms. The elevated value observed in comparison to a *cs* lattice can be attributed to the variance in drug entrapment within a *bcc* lattice, coupled with the absence of drug release outside the device. It is also noteworthy that the quantity of drug trapped indefinitely is not influenced by the system's geometry, which is in stark contrast to the behavior observed with a simple cubic lattice. Furthermore, it has been noted that scaling effects significantly influence the outcomes when simulations are conducted within a cylindrical matrix. This particular matrix, possessing the smallest area-to-volume ratio, demonstrates that scaling up can improve the fit of the data. This enhancement aids in elucidating the process of drug release from an inert and porous matrix through a Fickian diffusion mechanism. The results of this study suggest that utilizing the Monte Carlo simulation to model an inert and porous matrix within a *bcc* lattice provides a reliable method for elucidating the dynamics of drug release from delivery systems. This approach aids in comprehending how transport phenomena contribute to the process, thereby enabling the prediction of key design factors that influence the rate of drug release.

Acknowledgements

R.V.G. acknowledges the financial support through the Programa Interno de Cátedras de Investigación 2024 FESC UNAM under Grant Number CI2462. S.J.J. acknowledges for the fellowship 314168 from CONAHCYT previously received and who is a doctoral student from Programa de Doctorado en Ciencias Químicas, Universidad Nacional Autónoma de México (UNAM). J.G.M.H. also acknowledges for the fellowship 1313023 received from CONAHCYT.

References

1. Langer, R. *Science.* **1990**, *249*, 1527–1533. DOI: https://doi.org/10.1126/science.2218494.
2. Linares, V.; Casas, M.; Huwyler, J.; Caraballo, I. *J. Drug. Deliv. Sci. Technol.* **2023**, *90*, 105099. DOI: https://doi.org/10.1016/j.jddst.2023.105099.
3. Singh, M.; Shirazian, S.; Ranade, V.; Walker, G.; Kumar, A. *J. Powder Technol.* **2022**, 403. DOI: https://doi.org/10.1016/j.powtec.2022.117380.
4. Adembri, C.; Novelli, A.; Nobili, S. *Antibiotics.* **2020**, *9*, 676. DOI: https://doi.org/10.3390/antibiotics9100676.
5. Li, M.; Liu, R.-R.; Lü, L.; Hu, M.-B.; Xu, S.; Zhang, Y.-C. *Phys. Rep.* **2021**, *907*, 1–68. DOI: https://doi.org/https://doi.org/10.1016/j.physrep.2020.12.003.
6. Liao, J.; Hou, B.; Huang, H. *Carbohydr. Polym.* **2022**, *283*, 119177. DOI: https://doi.org/https://doi.org/10.1016/j.carbpol.2022.119177.
7. Quesada-Pérez, M.; Alberto, M.; Ramos, M.; Martin-Molina, A. *Macromol.* **2022**, *55*. DOI: https://doi.org/10.1021/acs.macromol.1c02178.

J. Mex. Chem. Soc. **2025**, *69*(1)
Special Issue

ISSN-e 2594-0317

8. Dan, N. *Colloids Surf. B Biointerfaces.* **2015**, *126*, 80–86. DOI: https://doi.org/https://doi.org/10.1016/j.colsurfb.2014.11.042.
9. Kaoui, B. *Eur. Phys. J. E.* **2018**, *41*, 20. DOI: https://doi.org/10.1140/epje/i2018-11626-7.
10. Martinez, L.; Villalobos, R.; Sánchez, M.; Cruz, J.; Ganem, A.; Melgoza, L. *Int. J. Pharm.* **2008**, *369*, 38–46. DOI: https://doi.org/10.1016/j.ijpharm.2008.10.023.
11. Villalobos, R.; Garcia, E.; Quintanar, D.; Young, P. *Curr. Drug Delivery* **2016**, *13*. DOI: https://doi.org/10.2174/1567201813666160512145800.
12. Stevens, D. R.; Downen, L. N.; Clarke, L. I. *Phys. Rev. B.* **2008**, *78*, 5425. DOI: https://doi.org/10.1103/PhysRevB.78.235425.
13. Zukowski, P.; Okal, P.; Kierczynski, K.; Rogalski, P.; Bondariev, V.; Pogrebnjak, A. *Energies (Basel.* **2023**, *16*, 8024. DOI: https://doi.org/10.3390/en16248024.
14. Villalobos, R.; Viquez, H.; Hernández, B.; Ganem, A.; Melgoza, L. M.; Young, P. M. *Pharm Dev. Technol.* **2012**, *17*, 344–352. DOI: https://doi.org/10.1016/j.ijpharm.2007.10.036.
15. Stauffer, D.; Aharony, A. in: *Introduction To Percolation Theory: Second Edition,* 2nd Ed. Taylor & Francis, 1992. DOI: https://doi.org/10.1201/9781315274386.
16. Queiroz, A. L.; Faisal, W.; Devine, K.; Garvie-Cook, H.; Vucen, S.; Crean, A. *Powder Technol.* **2019**, 354. DOI: https://doi.org/10.1016/j.powtec.2019.05.027.
17. Fernández-Hervás, M. J.; Vela, M. T.; Holgado, M. A.; del Cerro, J.; Rabasco, A. M. *Pharm. Acta Helv.* **1995**, *113*, 39–45. DOI: https://doi.org/https://doi.org/10.1016/0378-5173(94)00173-3.
18. Khizer, Z.; Nirwan, J.; Conway, B.; Ghori, M. *Int. J. Biol. Macromol.* **2020**, *155*, 835-845. DOI: https://doi.org/10.1016/j.ijbiomac.2020.03.227.
19. Kimura, G.; Puchkov, M.; Betz, G.; Leuenberger, H. *Pharm. Dev. Technol.* **2007**, *12*, 11–19. DOI: https://doi.org/10.1080/10837450601166494.
20. Draksler, P.; Mikac, U.; Laggner, P.; Paudel, A.; Janković, B. *Acta Pharm. (Warsaw, Pol.)***2021**, *71*, 215–243. DOI: https://doi.org/10.2478/acph-2021-0018.
21. Bonny, J. D.; Leuenberger, H. *Pharm. Acta Helv.* **1991**, *66*, 160–164. DOI: https://doi.org/10.3109/10837450.2010.542162.
22. Wenzel, T.; Stillhart, C.; Kleinebudde, P.; Szepes, A. *Drug Dev. Ind. Pharm.* **2017**, *43*, 1265–1275. DOI: https://doi.org/10.1080/03639045.2017.1313856.
23. Galdón, E.; Millán-Jiménez, M.; Mora-Castaño, G.; de Ilarduya, A. M.; Caraballo, I. *Pharmaceutics*. **2021**, *13*,7. DOI: https://doi.org/10.3390/pharmaceutics13071057.
24. Aguilar-de-Leyva, Á.; Gonçalves-Araujo, T.; Daza, V.; Caraballo, I. *Pharm. Dev. Technol.* **2014**, *19*,728-734. DOI: https://doi.org/10.3109/10837450.2013.829091.
25. Grund, J.; Körber, M.; Walther, M.; Bodmeier, R. *Int. J. Pharm.* **2014**, *469*. DOI: https://doi.org/10.1016/j.ijpharm.2014.04.033.
26. Wegner, T. I.; Peterson, M. C. in: *The Waite Group's Fractal Creations: Explore the Magic of Fractals on Your PC*, 1st ed.; Waite Group Press: Mill Valley, CA, 1991.
27. Ou, X. *Mater. Sci. Technol.* **2017**, *33*, 822–835. DOI: https://doi.org/10.1080/02670836.2016.1204064.
28. Cornette, V.; Ramirez-Pastor, A. J.; Nieto, F. *Phys. A (Amsterdam, Neth.)* **2003**, *327*, 71–75. DOI: https://doi.org/https://doi.org/10.1016/S0378-4371(03)00453-9.
29. Kurrer, C.; Schulten, K. *Phys. Rev. E* **1993**, *48*, 614–617. DOI: https://doi.org/10.1103/PhysRevE.48.614.
30. Lorenz, C. D.; May, R.; Ziff, R. M. *J. Stat. Phys.* **2000**, *98*, 961–970. DOI: https://doi.org/10.1023/A:1018648130343.
31. Villalobos, R.; Ganem, A.; Cordero, S.; Vidales, A. M.; Domínguez, A. *Drug Dev. Ind. Pharm.* **2005**, *31*, 535-543.
32. Bruce, A. D.; Jackson, A.; Ackland, G.; Wilding, N. *Phys. Rev. E.* **2000**, *61*, 906–919. DOI: https://doi.org/10.1103/PhysRevE.61.906.

J. Mex. Chem. Soc. **2025**, *69*(1)
Special Issue

ISSN-e 2594-0317

33. S Szortyka, M. M.; Girardi, M.; Fiore, C. E.; Henriques, V. B.; Barbosa, M. C. in: *Polymorphism in Lattice Models. In Advances in Chemical Physics*; Stanley, H. E., Ed.; Wiley, 2013; 152, 385–398. DOI: https://doi.org/10.1002/9781118540350.ch15.
34. Underwood, T. L.; Ackland, G. *J. Phys. Conf. Ser.* **2014**, 640. DOI: https://doi.org/10.1088/1742-6596/640/1/012030.
35. Maghsoodi, M.; Barghi, L. *Adv. Pharm. Bull.* **2011**, *1*, 27–33. DOI: https://doi.org/10.5681/apb.2011.004.
36. Gonçalves-Araújo, T.; Rajabi-Siahboomi, A.; Caraballo, I. *AAPS PharmSciTech,* **2010**, *11*, 558–562. DOI: https://doi.org/10.1208/s12249-010-9408-x.
37. Mason, L.; Campiñez, M. D.; Pygall, S. R.; Burley, J.; Gupta, P.; Storey, D. E.; Caraballo, I.; Melia, C. *Eur. J. Pharm. Bio*. **2015**, *94*, 485–492. DOI: https://doi.org/10.1016/j.ejpb.2015.06.019.
38. Misra, P. in: *Physics of Condensed Matter*; Academic Press, **2011**.
39. Bunde, A.; Havlin, S.; Nossal, R.; Stanley, H. E.; *J. Chem. Phys.* **1985**, *83*, 5909–5913. DOI: https://doi.org/10.1063/1.449622.
40. Sales, J. L.; Uñac, R. O.; Gargiulo, M. V; Bustos, V.; Zgrablich, G. *Langmuir.* **1996**, *12*, 95–100. DOI: https://doi.org/10.1021/la940859s.
41. Kosmidis, K.; Argyrakis, P.; Macheras, P. *J. Chem. Phys.* **2003**, *119*, 6373–6377. DOI: https://doi.org/10.1063/1.1603731.
42. Reynolds, T. D.; Mitchell, S. A.; Balwinski, K. M. *Drug Dev. Ind. Pharm.* **2002**, *28*, 457–466. DOI: https://doi.org/10.1081/DDC-120003007.
43. Mazur geb. Windolf, H.; Chamberlain, R.; Quodbach, *J. Pharm. (London, U. K.)* **2021**, *13*, 1453. DOI: https://doi.org/10.3390/pharmaceutics13091453.
44. P, N. R.; K, P.; T, R. R.; Reddy, B. C. S.; V, S.; M, L. N. *Int. J. Pharm. Sci. Nanotechnol.* **2010**, *3*, 872–876. DOI: https://doi.org/10.37285/ijpsn.2010.3.1.11.
45. Goyanes A.; Martínez, P.R.; Buanz, A.; Basit, A.W.; Gaiford, S. *Int. J. Pharm***. 2015**, *494*, 657-66. DOI: https://doi.org/10.1016/j.ijpharm.2015.04.069.
46. Golovnev, A.; Suss, M. E. *J. Chem. Phys.* **2018**, *149*, 144904. DOI: https://doi.org/10.1063/1.5041326.
47. Grest, G.; Cohen, M. *Adv. Chem. Phys.* **2007**, *48*, 455–525. DOI: https://doi.org/10.1002/9780470142684.ch6.
48. Cohen, M. H.; Turnbull, D. *J. Chem. Phys.* **1959**, *31*, 1164–1169. DOI: https://doi.org/10.1063/1.1730566.
49. Sykes, M. F.; Essam, J. W. *Phys. Rev.* **1964**, *133*, A310–A315. DOI: https://doi.org/10.1103/PhysRev.133.A310.
50. D S Gaunt; M F Sykes. *J. Phys. A. Math. Gen.* **1983**, *16*, 783. DOI: https://doi.org/10.1088/0305-4470/16/4/016.
51. Adler, J.; Meir, Y.; Aharony, A.; Harris, A. B.; Klein, L. *J. Stat. Phys.* **1990**, *58*, 511–538. DOI: https://doi.org/10.1007/BF01112760.
52. Lorenz, C. D.; Ziff, R. M. *Phys. Rev. E*. **1998**, *57*, 230–236. DOI: https://doi.org/10.1103/PhysRevE.57.230.
53. Zhang, J.; Cui, S. *Axioms.* **2023**, *12*, 481. DOI: https://doi.org/10.3390/axioms12050481.
54. Leuenberger, H.; Bonny, J. D.; Kolb, M. *Int. J. Pharm*. **1995**, *115*, 217–224. DOI: https://doi.org/10.1016/0378-5173(94)00266-8.
55. Wei, Z.; Yu, J.; Lu, Y.; Han, J.; Wang, C.; Liu, X. *Mater. Des.* **2021**, *198*, 109287. DOI: https://doi.org/https://doi.org/10.1016/j.matdes.2020.109287.
56. Van der Marck, S. *Int. J. Mod. Phys. C.* **1998**, *9*, 4,529-240. DOI: https://doi.org/10.1142/S0129183198000431.
57. Lundow, P.; Markstrom, K.; Rosengren, A. *Philos. Mag.* **2009**, *89*, 2009–2042. DOI: https://doi.org/10.1080/14786430802680512.
58. Vazquez, G. J. *Rev. Mex. Fis.* **1990**, *36*, 572–578.

J. Mex. Chem. Soc. **2025**, *69*(1)
Special Issue

ISSN-e 2594-0317

59. Jorgensen, W. L.; Duffy, E. M. *Bioorg. Med. Chem. Lett.* **2000**, *10*, 1155–1158. DOI: https://doi.org/https://doi.org/10.1016/S0960-894X(00)00172-4.
60. Makarov, V. A.; Andrews, B. K.; Smith, P. E.; Pettitt, B. M. *Biophys. J.* **2000**, *79*, 2966–2974. DOI: https://doi.org/https://doi.org/10.1016/S0006-3495(00)76533-7.
61. Yin, X.; Li, H.; Guo, Z.; Wu, L.; Chen, F.; Matas, M.; Shao, Q.; Xiao, T.; York, P.; He, Y.; Zhang, J. *AAPSJ*, **2013**, *15*. DOI: https://doi.org/10.1208/s12248-013-9498-y.